ACS APPLIED MATERIALS & INTERFACES

Surfaces, Interfaces, and Applications

Non-Passivated Silicon Anode Surface

Yanli Yin, Elisabetta Arca, Luning Wang, Guang Yang, Manuel Schnabel, Lei Cao, Chuanxiao Xiao, Hongyao Zhou, Ping Liu, Jagjit Nanda, Glenn Teeter, Bryan W. Eichhorn, Kang Xu, Anthony K. Burrell, and Chunmei Ban

ACS Appl. Mater. Interfaces, **Just Accepted Manuscript** • DOI: 10.1021/acsami.0c03799 • Publication Date (Web): 15 May 2020

is published by the American Chemical Society. 1155 Sixteenth Street N.W., Washington, DC 20036

Non-Passivated Silicon Anode Surface

*Yanli Yin[1], Elisabetta Arca[1]†, Luning Wang[2], Guang Yang[3], Manuel Schnabel[1]†, Lei Cao[1]‡, Chuanxiao Xiao[1], Hongyao Zhou[4], Ping Liu[4], Jagjit Nanda[3], Glenn Teeter[1], Bryan Eichhorn[2], Kang, Xu[5], Anthony Burrell[1] and Chunmei Ban[6] **

1, National Renewable Energy Laboratory, Golden, CO, USA.

2, University of Maryland, College Park, MD, USA

3, Oak Ridge National Laboratory, Oak Ridge, TN, USA

4, University of California San Diego, San Diego, CA, USA.

5, Army Research Laboratory, Adelphi, MD, USA

6, University of Colorado Boulder, Boulder, CO, USA

KEYWORDS: solid electrolyte interphase, silicon anode, carbonate electrolytes, surface and lithium ion battery.

ABSTRACT

A stable solid-electrolyte interphase (SEI) has been proven to be a key enabler to most advanced battery chemistries, where the reactivity between electrolyte and the anode operating beyond electrolyte stability limits must be kinetically suppressed by such SEI. The graphite anode used in state-of-the-art Li-ion batteries (LIBs) presents the most representative SEI example. Due to the similar operation potentials between graphite and silicon (Si), a similar passivation mechanism has been thought to apply on Si anode when using the same carbonate-based electrolytes. In this work, we found that the chemical

formation process of a proto-SEI on Si is closely entangled with incessant SEI decomposition, detachment and reparation, which lead to continuous lithium consumption. Using a special galvanostatic protocol designed to observe the SEI formation prior to Si lithiation, we were able to deconvolute the electrochemical formation of such dynamic SEI from the morphology and mechanical complexities of Si, and showed that a pristine Si anode could not be fully passivated in carbonate-based electrolytes.

INTRODUCTION

Solid electrolyte interphase (SEI) is required to kinetically stabilize the reversibility of advanced batteries, where the electrodes usually operate beyond the thermodynamic stability limits of electrolytes.[1, 2] Such SEI insulates electrons but conducts ions of the cell reaction, such as Li^+ in lithium ion batteries (LIBs).[3-5] Since graphite has been used as standardized anode in LIBs for nearly 3 decades, the chemical and electrochemical behavior of SEI thereon has been extensively investigated, [6-8] using diverse advanced characterization techniques —attenuated total reflection-Fourier transform infrared spectroscopy (ATR-FTIR),[9] nuclear magnetic resonance spectroscopy (NMR),[10] X-ray photoelectron spectroscopy (XPS),[11] X-ray reflectivity,[12] scanning spreading-resistance microscopy (SSRM) resistance imaging,[13] frequency generation vibrational spectroscopy (SFG-VS)[14] and thermogravimetric analysis (TGA).[15] These studies painted a general picture of SEI being multilayer-structured and composed of lithium fluoride, carbonates and alkylcarbonates as the main components.[16, 17] Since Si operates in a similar potential range as graphite (0.40 V vs. Li for Si, 0.1 V vs. Li for graphite), the above fundamental information regarding SEI was believed to be applicable to Si anode as long as the same carbonate-based electrolytes are used.[18]

However, unlike graphite,[19] Si anodes experience large volumetric and morphological changes during cycling [20-23]. This major characteristic brought by its alloy/dealloy nature leads to physical disintegration (cracks and fragmentations) that creates “new” Si surfaces being exposed to the

electrolyte and requiring "new" SEI formation.[24] Therefore, when SEI on Si is studied, its intrinsic chemical and electrochemical behavior were always entangled with the ever evolving surface morphology.[25]

To decouple the intrinsic electrochemical behavior of Si-SEI from the morphology changes occurring simultaneously, we focus on the formation and chemistry of SEI before lithiation occurs in Si anodes, hence excluding the interference from the alloy/dealloy of Si. Here, we define the SEI formed before lithiation as the "proto-SEI (p-SEI)". Surprisingly, we found that the surface of Si anode remains reactive even after hundreds of cathodic processes; and the constituents of SEI experience dynamic changes with simultaneous detachment and reformation. The chemical instability and reparation of Si SEI suggest that it is impossible to stabilize a pristine Si anode in carbonate-based electrolytes. Alternative electrolyte formulations must be explored to enable Si anodes in practical cells.

RESULTS AND DISCUSSION

Electrochemistry and morphology of p-SEI. Different cut-off voltages were adopted during the galvanostatic charge/discharge of the half cells consisting of Si as working and Li metal as counter electrodes (Figure 1). Figure 1 (a1) shows the voltage profiles in the first 20 cycles, while Figure 1 (a2) zooms the first lithiation process in, with differential capacity plotted in Figure 1 (a3). The lithiation process was set for 2 hours. A typical first lithiation process was observed for the crystalline Si anode.[14] Based on the three peaks shown in Figure 1 (a3), the lithiation (cathodic) process can be divided into three regimes—Regime 1 represents the electrochemical activities above 400 mV, Regime 2 between 400 and 115 mV, and Regime 3 the lithiation in Si anodes, which occurs below 115 mV. The reactions occurring in Regime 1 and 2 are related to the reduction of electrolyte and other irreversible processes related to the SEI formation, which are the focus of this study. The plateau corresponds to the crystalline-to-amorphous phase transition.[26] By precisely confining the low cut-off voltages, such as 400 mV and 115 mV, we can deconvolute the formation of p-SEI without involving the mechanical and morphological complexities induced by lithiation and delithiation of the silicon. A 1-hour (when using a cut-off voltage of 400mV) or a 3-hour rest period (when using a cut-off voltage of 115mV) is applied to

the Si anode after the designed cathodic process. So, each electrochemical cycle includes a cathodic process followed by a rest period. A 10-hour rest was then applied every 20 cycles, for the SEI evolution during this longer rest time to be monitored. Figure 1 (b1, b2, b3) and Figure 1 (c1, c2, c3) reflect the effect cast by the cut-off voltages of 400 mV and 115 mV, respectively.

At 400 mV cut-off voltage, the magnitude of the differential capacity decreases with increasing cycles (Figure 1 (b3)), which indicates that the parasitic reactions in Regime 1 (above 400 mV) diminish while Si surface stabilizes against the electrolyte in this voltage range. However, when a 10-hour long rest was introduced after the cathodic process—between the 20^{th} and 21^{st} cycle, or between the 40^{th} and 41^{st} cycle, the Si surface resumes reactivity (Figure 1 (b3)). Although there was no current or potential polarization applied during the 10-hour rest period, the formed SEI somehow ceased to passivate Si surface.

When Si anode was polarized to a lower cut-off voltage of 115 mV (Regime 2), the voltage profiles and the differential capacity now include the electrochemical behavior already observed in Regime 1 along with new processes related to Si lithiation (Figure 1 (c2 and c3)). Compared with the reactivity in Regime 1, the reactions in Regime 2 are more pronounced because more electrons are involved. The Si surface remains active even after the repeated 40 cathodic processes. During the 10-hour rest period between the 20^{th} and 21^{st} cycle, or between the 40^{th} and 41^{st} cycle, the surface becomes more reactive, similar to what was observed for Regime 1 with the 400-mV cut-off. The surface reactivation suggests that certain components in the formed SEI evolve during the rest periods and fail to protect the Si surface from further reaction with the electrolytes. Note that there is no anodic process after the cathodic process, and no current or potential was applied to accelerate/initialize any reaction after the cathodic process.

Figure 2 counts electrons involved in the reactions in both Regime 1 and 2. To make the plot more legible, we only plotted the data every 10 cycles plus two more data points after each 10-hour rest. Apparently, the reduction reaction at the surface of the Si anodes never completely stopped during the 100 cycles, even when the low cut-off limit was high (400 mV, Regime 1). Moreover, the spikes

following every 10-hour rest indicate that the Si surface became more reactive during the rest. It strongly implies that the products from the parasitic reactions in Regime 1 and 2 constantly evolve, and the passivation provided by the formed SEI eventually fall apart. These parasitic reactions in both Regime 1 and 2 would continuously consume Li^+.

The surface morphology of Si anodes harvested from the aforementioned cathodic process was examined using scanning electron microscopy (SEM), which produces the images of pristine Si (Figure 3a), Si anode after experiencing Regime 1 reactions (Figure 3b), Regime 2 reactions (Figure 3c), and the 10-hour rest (Figure 3d). As expected, no mechanical cracks were observed in all of the Si anodes, and the smooth morphology remains as long as Si potential was confined above 400 mV. However, Si surface becomes rough when its potential approaches 115 mV. The most interesting observation is that the surface morphology changes after the 10-hour rest (Figure 3d), indicating partial removal of some of SEI components. In fact, we observed that the Si surface became reactivated after the rest period.

Chemistry of p-SEI. The non-passivating nature of p-SEI stems from its chemistry. Angular-resolved surface-sensitive XPS with different take-off angles was used to investigate the chemistry and composition along depth direction. At the grazing exit angle of 5 degree, the very top layer (0.5-2 nm, depending on the inelastic mean free path of the various elements considered) should be revealed; at 45 degree a probing-depth up to 4-6 nm, could be achieved, while at 85 degree the whole probing-depth (up to 6-10 nm) should be reflected.

Formation of both organic and inorganic components are revealed on the Si surface recovered from Regime 1 process (Figure 4). Here peak fitting for each core-level was conducted to determine components of p-SEI. In addition, for Si, a tabulated value of 0.61 spin orbit splitting was implemented in the fitting procedure. Identification of the various chemical compounds was possible because element cores belonging to the same chemical compound have a characteristic binding energy separation, which acts as a fingerprint to mark that species. Charging and differential charging effects can make interpretation of XPS data elusive. For our samples, the charging effect only induces the peak shift. Based our previous study, if the charging effect is not severe, for a given chemical compound, all the

elements present in it should be charging to the similar extent, and thus, the core levels of the elements in those compounds will be shifted to higher binding energy by the similar amount.[28] Thus, attribution based on the relative position of core levels (Δ_{BE}) serves as a more accurate quantification than attribution based on absolute position. To establish the Δ_{BE} for compounds and functional groups that can potentially being present in the SEI, we did a thorough literature research, and tabulated the average Δ_{BE} for the various groups and chemical assignment in Table S1.

As this identification method is not affected by charging effects,[28] no correction was applied to the binding energy scale. The analysis of the C 1s core levels confirms that carbonate groups (CO_3) at 292 eV, ester groups (O-C=O) at 290-291 eV, ether (C-O) at 288-289 eV, and aliphatic (C-C/C-H) at 286-287 eV are all present after the cathodic process down to 400 mV. The O 1s spectra includes the peaks at 535 eV and 533 eV indicating the existence of C=O and C-O bonds, respectively, which is consistent with the carbonate/ester and ethers suggested by C 1s spectra. The appearance of the carbonate functional groups suggests the existence of organic carbonates such as lithium ethylene di-carbonate (LiEDC), lithium ethylene mono-carbonate (LiEMC) as well as inorganic carbonates such as Li_2CO_3 after the reactions in Regime 1. The information from Raman spectroscopy further confirmed the co-existence of both organic alkyl carbonates and lithium carbonates (Figure S1). The reaction scheme of LiEDC formation from ethylene carbonate (EC) reduction has been well studied and verified,[16, 17] while recent research identified LiEMC as a major SEI components, probably originating from LEDC via a mechanism still not well understood.[29] Based on the F 1s spectra, LiF at 686-687 eV also constitutes to part of p-SEI, supported by the vast majority of the fluorine signal, which might be generated via both chemical and electrochemical processes.[8] $LiPF_6$ at 689-690 eV is also present in trace quantity, probably due to electrolyte residue at the Si electrode.[11] Judged from the Si 2p spectra, p-SEI appears to be a relatively thin layer, as the signal of the SiO_x below it (104-105 eV) and the Si substrate (~100 eV) are still visible even on the most surface-sensitive measurements at 5°.[11] Li 1s spectrum yields a broad peak at 57-58 eV which can be assigned to the combination to LiF and $LiPF_6$ and Li carbonate species.[27]

The p-SEI continuously grows and becomes thicker in Regime 2 (Figure 5, and Figure S1), with the underlying SiO_x/Si gradually disappearing in the most surface sensitive measurements (5°) or much more attenuated in the more depth-probing measurements—using a take-off exit angle of 85 degrees. Qualitatively, p-SEI differs in composition as well: the organic components appear gradually prevail and the number of carbonates and ester species is much higher in comparison to the Si anodes after Regime 1. This effect is quantified in Table S2. LiF and trace $LiPF_6$ remain present in p-SEI after experiencing Regime 2.

XPS depth profiling (Figure 6) displays the progression of the chemical species from surface into the bulk of p-SEI, confirming the existence of SiO_x before elemental Si from the substrate. Li 1s profile (Figure 6b) reveals that, at least within the detection limit of the measurements, the Si remains un-lithiated, further confirming that the rigorous cut-off voltage protocol adopted here indeed ensures the effective exclusion of interference from Si lithiation/de-lithiation.

Stability of p-SEI. After the cathodic process down to 115 mV, the voltage response during a prolonged rest period (40 hours) is recorded (Figure 7a). Surprisingly, the voltage exhibits a plateau around 1.3 V before increasing to 2.0 V, which is especially visible in the differential plot (inset, Figure 7a). We believe that some SEI components might be experiencing a chemical reaction during the rest, which is reflected by such plateau.

Among the SEI constituents (LiF, Li_2CO_3, LiEDC and/or LiEMC), lithium alkylcarbonates are the primary suspect because of its well-known sensitivity. To verify this suspicion, we synthesized both LiEDC and LiEMC, which have been established as the most probable alkylcarbonates in SEI [29], and tested their electrochemical stability in electrolytes by assembling these pure alkylcarbonates into cells. Figure 7b compares the voltage responses during the 40-hour rest for the LiEDC electrode and the Cu-foil used as the control sample. LiEDC displays a short plateau around 1.1 V (inset of Figure 7b), before reaching 1.8 V. The difference between LiEDC and Cu is negligible if the difference between the surface areas of Cu and LiEDC is considered LiEMC electrode, however, very surprisingly shows a rather reactive behavior in ethylene carbonate (EC)-based electrolyte as evidenced by its cyclic

voltammetry (CV). To eliminate the possibility that this reaction is related to EC itself, we also ran a parallel test of LiEMC in propylene carbonate-based electrolyte (Figure 7c and 7d), where multiple redox peaks between 1.0 and 4.5 V were detected. In contrast to the redox activities of LiEMC, the control sample—the Pt electrode—remains inert in the entire voltage range. Although the CV protocol is different from the galvanostatic process used for Si electrodes, Figure 7c and 7d unambiguously prove that the LiEMC may not be stable against these cyclic carbonates used in the LIBs' electrolyte, involving the complicate redox reactions within the Li-ion battery operation window.

The angle-resolved XPS spectra have been used again here to compare the surface chemistry before and after 10-hour rest period. The peaks attributed to carbonate/ester group species are significantly reduced after the rest (Figure 8), suggesting that those carbonates no longer exist in the p-SEI on the Si surface. The solubility of both Li_2CO_3 and LiEDC salts in carbonate solvents is low,[30] and can be enhanced at elevated termpature.[31] With the insights from electrochemical analysis (Figure 7), we believe that some semi-carbonates decompose and may have been oxidized, as shown by a recent work for LiEDC.[8] There is a high chance that LiEMC may experience similar redox reactions too. However, p-SEI after the rest remains thicker in comparison to p-SEI formed in the Regime I, as evidenced by the fact that the signal of the underlying Si-layer is not detectable for the samples measured at grazing exit and substantially attenuated at an exit angle of 85 degree. Overall, due to its own chemical reactivity, the p-SEI formed from carbonate-based electrolytes only provides partial stabilization of Si at its lithiation potential, which is insufficient to fully passivate Si against parasitic reactions.

CONCLUSION

The coupled morphological-mechanical-electrochemical phenomena make it extremely hard to understand the intrinsic chemical and electrochemical properties of SEI via the standard electrochemical procedures. This work presents a new approach to deconvolute the contributions from electrochemical as well as mechanical and morphological processes that simultaneously occur during Si lithiation. We found that chemical components (such as LiEDC and/or LiEMC) in p-SEI formed from carbonate-based electrolytes are intrinsically reactive on Si surface. Hence, the interphase is unable to provide full

passivation as needed by reversible cycling of this high capacity anode materials. To make Si practical, one not only needs to address the volume change of Si during its alloy/dealloy process, but also has to seek after new electrolyte formulation that provide true kinetic stabilization of Si.

EXPERIMENTAL SECTION

1. The construction of anode half cells

The Si electrodes were Si wafers (Czochralski, boron-doped, 0.001-0.005 Ohm·cm, (100) orientation, 700 μm thick, purchased from Addison Engineering) that were laser-cut to an area of 1×1 cm^2, and then received an RCA clean [32] without the HF steps in order to maintain the native oxide film on the surface. After cleaning, the wafers were dried in vacuum oven at 100 °C prior to the cell fabrication. All further cell fabrication was performed in an Ar-filled glovebox (O_2 and H_2O < 0.5 ppm). There is a native oxide layer formed on the Si wafer surface.

The LiEDC electrodes were fabricated by pressing 1mg LiEDC powders on Cu foils. The LiEMC electrodes were fabricated by pressing LiEMC powders on 300 nm Pt coated stainless steel spacer. Both LiEDC and LiEMC materials were synthesized in the lab with the synthesis methods detailed in the reference.[29, 33]

The lithium foil was used as counter electrodes. The lithium foil was scratched by a sharp blade leading to an exposure of a shiny surface in an Ar-filled glovebox. The EC based electrolyte is 1.2 mol/L $LiPF_6$ dissolved in the solution comprised of ethylene carbonate (EC): ethyl methyl carbonate (EMC) with the weight ratio of 3:7. The PC based electrolyte is 1.2 mol/L $LiPF_6$ dissolved in the solution comprised of propylene carbonate solvent. All of the lithium salts and carbonate solvents for preparing of electrolytes were purchased from Tomiyama Pure Chemical Industries, LTD, without any further treatment. The electrolyte was used in every cell with the same volume of 7 μL. One piece of glass microfiber filter (Whatman, GE Healthcare Life Sciences) with the thickness of 260 μm and one piece of plastic film (2325, Celgard) with the thickness of 25 μm was punched to the round size with the area of 2.27 cm^2 and were stacked as the separator.

An O-ring sealed cell containing all above items was finally assembled in an Ar-filled glovebox, with O_2 and H_2O level less than 2 ppm. 1 piece of 1 mm-thick stainless-steel spacer and 1 piece of 0.3 mm-thick stainless-steel spring were used to keep every cell at a constant internal pressure.

2. The electrochemistry of p-SEI

The voltage profile was obtained from the cells by the galvanostatic testing (VMP3, Bio-Logic Science Instruments SAS).

3. The morphology characterization of p-SEI

The micro-structural morphology analysis of the p-SEI on Si anode surface was carried out by a SEM using a field-emission gun in the immersion-lenses mode (Nova 630, FEI).

4. The spectroscopic characterization of p-SEI

The composition of the p-SEI was determined using X-ray photoelectron spectroscopy (XPS) and Raman Scattering.

X-ray Photoelectron Spectroscopy was performed on the samples cycled at 400 mV cut-off voltage and no rest, 115 mV cut-off voltage and no rest and 115 mV cut-off voltage after the extra-long rest. After cycling, samples were gently washed in Dimethyl carbonate (DMC) for 2 minutes, dried in the vacuum chamber for 1 hour and immediately transferred into the XPS system via an air-free transfer mechanism. For the measurements, the PHY 5600 XPS system was used, which operates at a base pressure better than 9×10^{-10} torr, using a K-alpha Al source. Survey spectra were acquired for all samples to determine the elemental composition at the surface. Spectra for core-levels were acquired for each element in high resolution mode using 3 different exit angles: a shallow angle (~5 degrees with respect to the surface) was used to probe the first few nanometers of the sample, 45 degrees exit angle was used for the intermediate thicknesses whereas to probe deeper into the sample, 85 degrees exit angles was used. Data analysis was performed using a custom program adapted from Schmid et al.[34]

Prior to each Raman measurement, each sample was sealed in a customized Raman pouch cell in an Ar-filled glove box with O_2 <0.1 ppm and H_2O < 0.5 ppm. Raman spectrum of each sample was taken from a confocal micro-Raman system (WITec, 532 nm laser with local power < 1mW, exposure time =

10 s, number of scans = 20 and grating = 600 grooves/mm, 20× objective). The laser spot size is approximately 1 μm. The background reduction for each spectrum was performed using a WIRE 4.0 software package (Renishaw). The background of all spectra was reduced against the anchor points at the same frequency locations to assure consistent results.

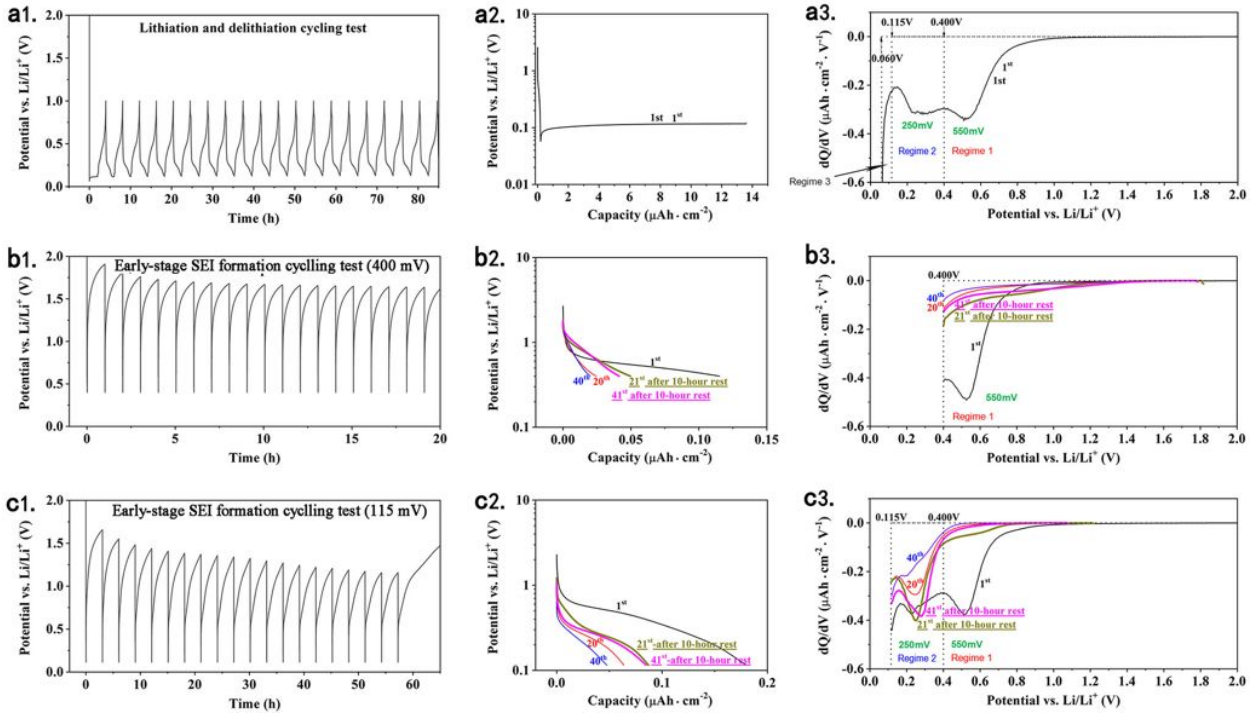

Figure 1. The voltage profile as the function of time (a1) and (a2) capacity and (a3) the differential capacity profile under the condition including both electrolyte reduction and Si lithiation. The voltage profile as the function of time (b1) and (b2) capacity and (b3) the differential capacity profile under the procedure (400 mV) including Regime 1, at the 1st, 20th, 21st after 10-hour rest, 40th and 41st cycle after 10-hour rest. The voltage profile as the function of time (c1) and (c2) capacity and (c3) the differential capacity profile under the procedure (115 mV) including both Regime 1 and Regime 2, at the 1st, 20th, 21st after 10-hour rest, 40th and 41st cycle after 10-hour rest.

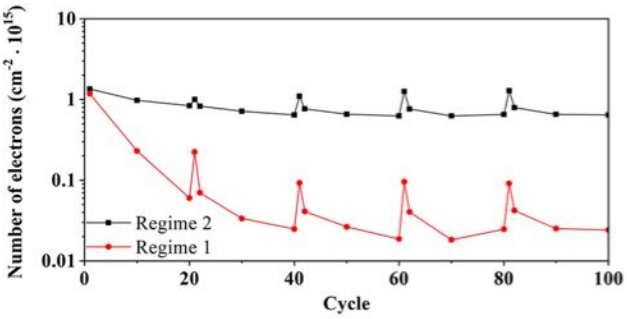

Figure 2. The number of electrons involved in the es-SEI formation as a function of cycle number for both Regime 1 (above 400 mV) and Regime 2 (between 115 mV and 400 mV).

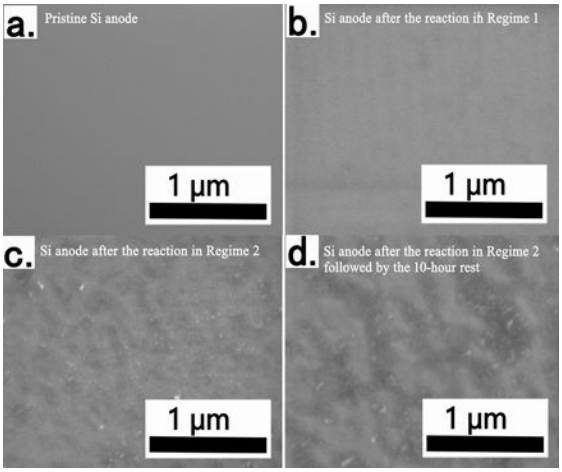

Figure 3. The SEM morphology of (a) the Si pristine surface, (b) the Si anode after the cathodic with the cut off potential of 400 mV and no rest, (c) the Si anode after the cathodic with the cut off potential of 115 mV and no rest, and (d) the Si anode after the cathodic with the cut off potential of 115 mV followed by a 10-hour rest.

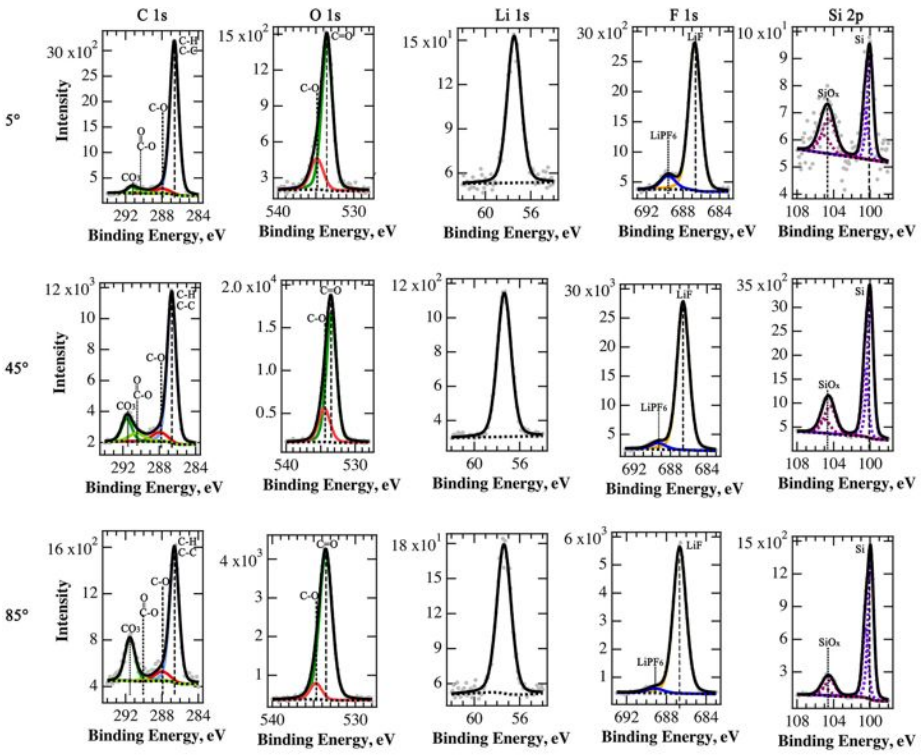

Figure 4. The XPS spectra obtained from the Si anode after the cathodic process followed by the rest period. The cut-off voltage for the cathodic process is 400 mV.

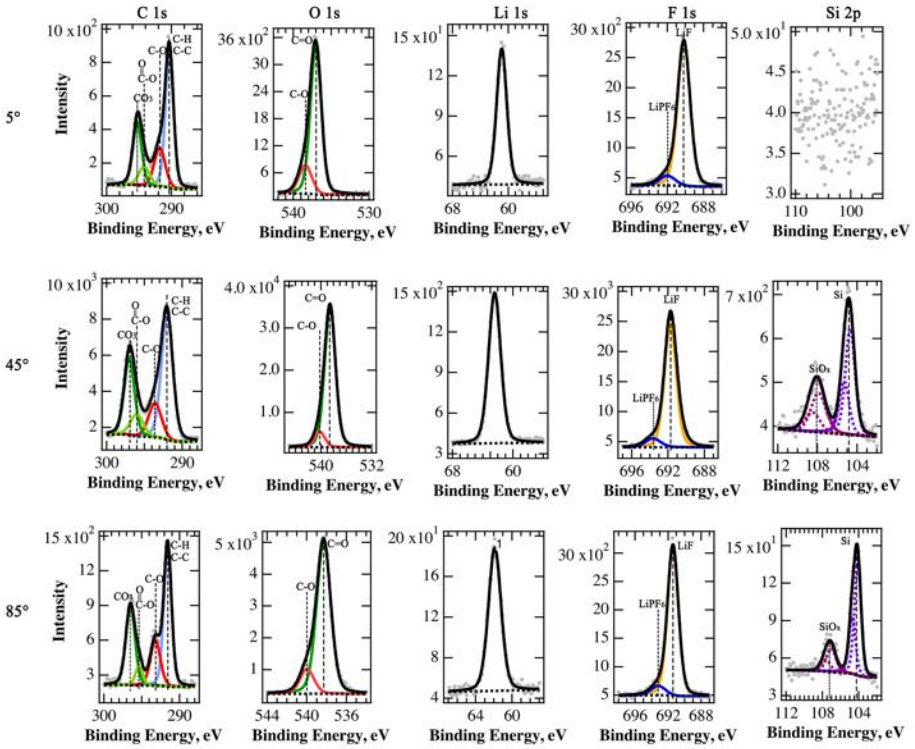

Figure 5. The XPS spectra obtained from the Si anode after the cathodic process. The cut-off voltage for the cathodic process is 115 mV (refer to Δ_{BE} in Table S1).

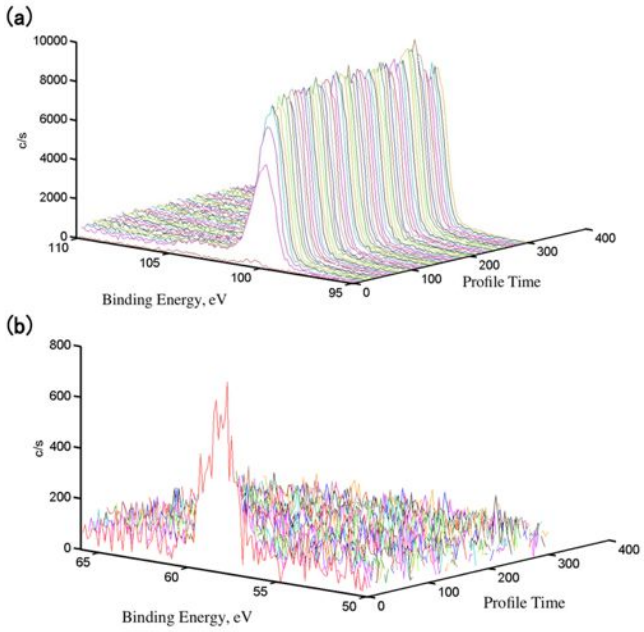

Figure 6. The XPS depth profile obtained from the Si anode after the cathodic process with a cut-off voltage of 115 mV. (a) Si 2p profile. (b) Li 1s profile.

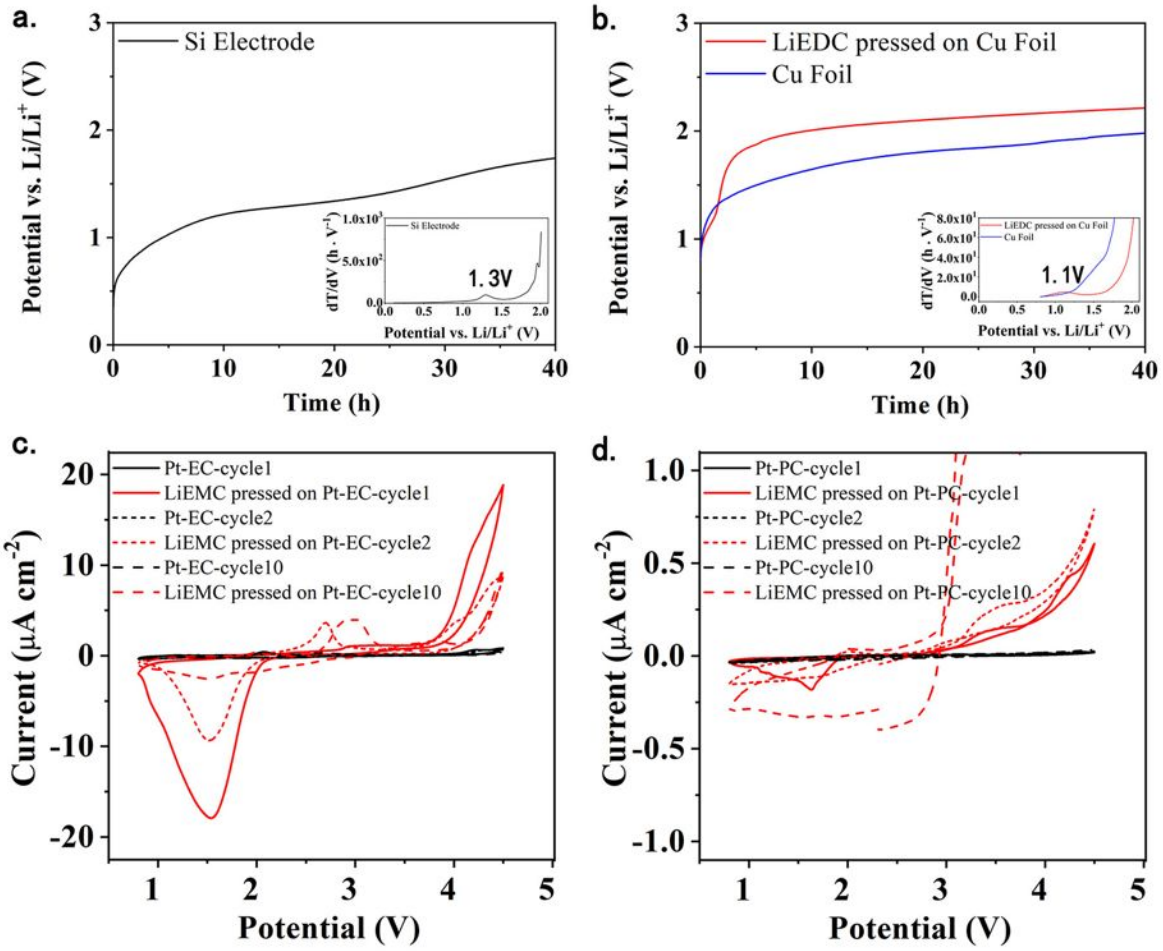

Figure 7. (a)The voltage profile of Si anode as a function of time and the differential time profile as the function of potential (insert) during a 40-hour rest; (b) The voltage profile of the LiEDC electrode and the Cu control electrode as a function of time and the differential time profile as the function of potential (insert) during a 40-hour; (c) The cyclic voltammetry profile (1st, 2nd and 10th cycle) of the Pt electrode and LiEMC electrode in the EC-based electrolyte; and (d) in the PC based electrolyte.

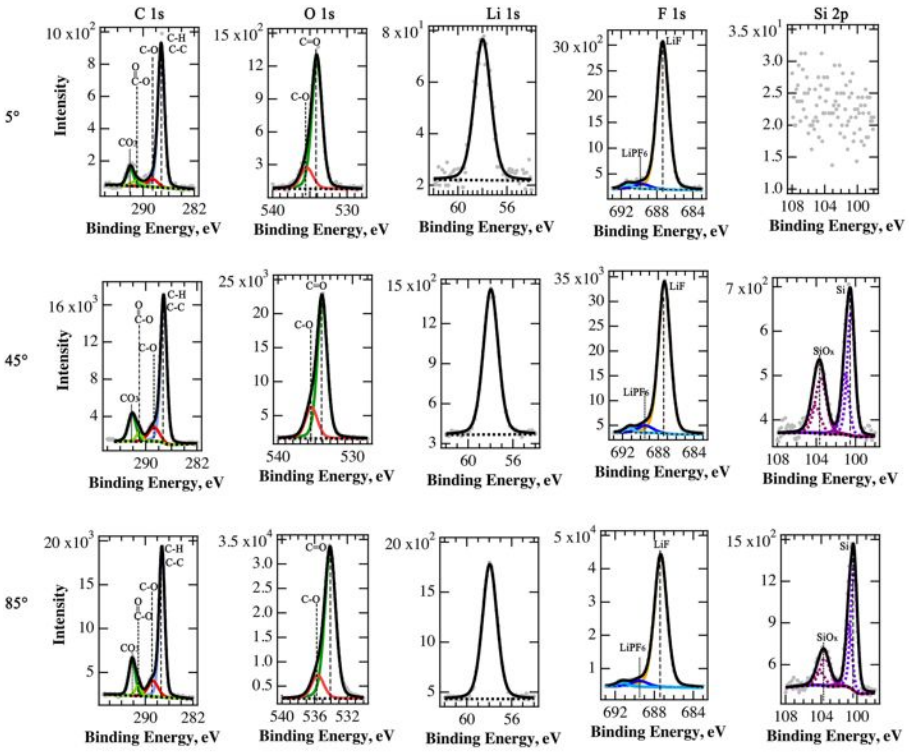

Figure 8. The XPS spectra obtained from the Si anode after the cathodic process followed by the rest period. The cut-off voltage for the cathodic process is 115 mV.

AUTHOR INFORMATION

Corresponding Author

*chunmei.ban@colorado.edu

Present Addresses

† Lawrence Berkeley National Laboratory, Berkeley, CA, USA

‡ Alphabet, Inc, Mountain View, CA, USA

Author Contributions

The manuscript was written through contributions of all authors. All authors have given approval to the final version of the manuscript.

Funding Sources

U.S. Department of Energy (DOE) under Contract No. DE-AC36-08GO28308.

ACKNOWLEDGMENT

This work was authored in part by Alliance for Sustainable Energy, LLC, the manager and operator of the National Renewable Energy Laboratory for the U.S. Department of Energy (DOE) under Contract No. DE-AC36-08GO28308. The research is supported by the Vehicle Technologies Office of the U.S. Department of Energy Office of Energy Efficiency and Renewable Energy, under the supervision of Brian Cunningham. The views expressed in the article do not necessarily represent the views of the DOE or the U.S. Government. The U.S. Government retains and the publisher, by accepting the article for publication, acknowledges that the U.S. Government retains a nonexclusive, paid-up, irrevocable, worldwide license to publish or reproduce the published form of this work, or allow others to do so, for U.S. Government

purposes. The research is partially supported by the Department of Paul M. Rady Mechanical Engineering and College of Engineering and Applied Sciences at University of Colorado Boulder.

Supporting Information. XPS and Raman data.

REFERENCES

(1) Xu, K. Electrolytes and Interphases in Li-Ion Batteries and Beyond. *Chem. Rev.* **2014**, *114*, 11503-11618.
(2) Hu, L.; Xu, K. Nonflammable Electrolyte Enhances Battery Safety. *Proc. Natl. Acad. Sci. U. S. A.* **2014**, *111*, 3205.
(3) Peled, E.; Menkin, S. Review—SEI: Past, Present and Future. *J. Electrochem. Soc.* **2017**, *164*, A1703 -A1719.
(4) Gauthier, M.; Carney, T. J.; Grimaud, A.; Giordano, L.; Pour, N.; Chang, H.-H.; Fenning, D. P.; Lux, S. F.; Paschos, O.; Bauer, C.; Maglia, F.; Lupart, S.; Lamp, P.; Shao-Horn, Y. Electrode–Electrolyte Interface in Li-Ion Batteries: Current Understanding and New Insights. *J. Phys. Chem. Lett.* **2015**, *6*, 4653-4672.
(5) Liu, Q.; Cresce, A.; Schroeder, M.; Xu, K.; Mu, D.; Wu, B.; Shi, L.; Wu, F. Insight on Lithium Metal Anode Interphasial Chemistry: Reduction Mechanism of Cyclic Ether Solvent and SEI Film Formation. *Energy Storage Mater.* **2019**, *17*, 366-373.
(6) Xu, K.; von Cresce, A.; Lee, U. Differentiating Contributions to "Ion Transfer" Barrier from Interphasial Resistance and Li+ Desolvation at Electrolyte/Graphite Interface. *Langmuir* **2010**, *26*, 11538-11543.
(7) Nie, M.; Abraham, D. P.; Seo, D. M.; Chen, Y.; Bose, A.; Lucht, B. L. Role of Solution Structure in Solid Electrolyte Interphase Formation on Graphite with LiPF6 in Propylene Carbonate. *J. Phys. Chem. C* **2013**, *117*, 25381-25389.
(8) Liu, T.; Lin, L.; Bi, X.; Tian, L.; Yang, K.; Liu, J.; Li, M.; Chen, Z.; Lu, J.; Amine, K.; Xu, K.; Pan, F. In Situ Quantification of Interphasial Chemistry in Li-ion Battery. *Nat. Nanotechnol.* **2019**, *14*, 50-56.
(9) Shi, F.; Ross, P. N.; Somorjai, G. A.; Komvopoulos, K. The Chemistry of Electrolyte Reduction on Silicon Electrodes Revealed by in Situ ATR-FTIR Spectroscopy. *J. Phys. Chem. C* **2017**, *121*, 14476-14483.

(10) Michan, A. L.; Leskes, M.; Grey, C. P. Voltage Dependent Solid Electrolyte Interphase Formation in Silicon Electrodes: Monitoring the Formation of Organic Decomposition Products. *Chem. Mater.* **2016**, *28*, 385-398.
(11) Philippe, B.; Dedryvère, R.; Allouche, J.; Lindgren, F.; Gorgoi, M.; Rensmo, H.; Gonbeau, D.; Edström, K. Nanosilicon Electrodes for Lithium-Ion Batteries: Interfacial Mechanisms Studied by Hard and Soft X-ray Photoelectron Spectroscopy. *Chem. Mater.* **2012**, *24*, 1107-1115.
(12) Cao, C.; Steinrück, H.-G.; Shyam, B.; Stone, K. H.; Toney, M. F. In Situ Study of Silicon Electrode Lithiation with X-ray Reflectivity. *Nano Lett.* **2016**, *16*, 7394-7401.
(13) Stetson, C.; Yoon, T.; Coyle, J.; Nemeth, W.; Young, M.; Norman, A.; Pylypenko, S.; Ban, C.; Jiang, C.-S.; Al-Jassim, M.; Burrell, A. Three-dimensional Electronic Resistivity Mapping of Solid Electrolyte Interphase on Si Anode Materials. *Nano Energy* **2019**, *55*, 477-485.
(14) Horowitz, Y.; Han, H.-L.; Ross, P. N.; Somorjai, G. A. In Situ Potentiodynamic Analysis of the Electrolyte/Silicon Electrodes Interface Reactions - A Sum Frequency Generation Vibrational Spectroscopy Study. *J. Am. Chem. Soc.* **2016**, *138*, 726-729.
(15) Yoon, T.; Milien, M. S.; Parimalam, B. S.; Lucht, B. L. Thermal Decomposition of the Solid Electrolyte Interphase (SEI) on Silicon Electrodes for Lithium Ion Batteries. *Chem. Mater.* **2017**, *29*, 3237-3245.
(16) Xu, K.; Zhuang, G. V.; Allen, J. L.; Lee, U.; Zhang, S. S.; Ross, P. N.; Jow, T. R. Syntheses and Characterization of Lithium Alkyl Mono- and Dicarbonates as Components of Surface Films in Li-Ion Batteries. *J. Phys. Chem. B* **2006**, *110*, 7708-7719.
(17) Shkrob, I. A.; Zhu, Y.; Marin, T. W.; Abraham, D. Reduction of Carbonate Electrolytes and the Formation of Solid-Electrolyte Interface (SEI) in Lithium-Ion Batteries. 1. Spectroscopic Observations of Radical Intermediates Generated in One-Electron Reduction of Carbonates. *J. Phys. Chem. C* **2013**, *117*, 19255-19269.
(18) Xu, C.; Lindgren, F.; Philippe, B.; Gorgoi, M.; Björefors, F.; Edström, K.; Gustafsson, T. Improved Performance of the Silicon Anode for Li-Ion Batteries: Understanding the Surface Modification Mechanism of Fluoroethylene Carbonate as an Effective Electrolyte Additive. *Chem. Mater.***2015**, *27*, 2591-2599.
(19) An, S. J.; Li, J.; Daniel, C.; Mohanty, D.; Nagpure, S.; Wood, D. L. The State of Understanding of the Lithium-ion-battery Graphite Solid Electrolyte Interphase (SEI) and Its Relationship to Formation Cycling. *Carbon* **2016**, *105*, 52-76.

(20) Son, S.-B.; Kappes, B.; Ban, C. Surface Modification of Silicon Anodes for Durable and High Energy Lithium-Ion Batteries. *Isr. J. Chem.* **2015**, *55*, 558-569.
(21) Wang, X.; Singh, S. S.; Ma, T.; Lv, C.; Chawla, N.; Jiang, H. Quantifying Electrochemical Reactions and Properties of Amorphous Silicon in a Conventional Lithium-Ion Battery Configuration. *Chem. Mater.* **2017**, *29*, 5831-5840.
(22) Son, S.-B.; Cao, L.; Yoon, T.; Cresce, A.; Hafner, S. E.; Liu, J.; Groner, M.; Xu, K.; Ban, C. Interfacially Induced Cascading Failure in Graphite-Silicon Composite Anodes. *Adv. Sci.* **2019**, *6*, 1801007.
(23) Shi, F.; Song, Z.; Ross, P. N.; Somorjai, G. A.; Ritchie, R. O.; Komvopoulos, K. Failure Mechanisms of Single-crystal Silicon Electrodes in Lithium-ion batteries. *Nat. Commun.* **2016**, *7*, 11886.
(24) Chew, H. B.; Hou, B.; Wang, X.; Xia, S. Cracking Mechanisms in Lithiated Silicon Thin Film Electrodes. *Int. J. Solids Struct.* **2014**, *51*, 4176-4187.
(25) Nie, M.; Abraham, D. P.; Chen, Y.; Bose, A.; Lucht, B. L. Silicon Solid Electrolyte Interphase (SEI) of Lithium Ion Battery Characterized by Microscopy and Spectroscopy. *J. Phys. Chem. C* **2013**, *117*, 13403-13412.
(26) Obrovac, M. N.; Christensen, L., Structural Changes in Silicon Anodes during Lithium Insertion/Extraction. *Electrochem. Solid-State Lett.* **2004**, *7*, A93 -A96.
(27) Parimalam, B. S.; Lucht, B. L. Reduction Reactions of Electrolyte Salts for Lithium Ion Batteries: LiPF6, LiBF4, LiDFOB, LiBOB, and LiTFSI. *J. Electrochem. Soc.* **2018**, *165*, A251 -A255.
(28) Wood, K. N.; Teeter, G. XPS on Li-Battery-Related Compounds: Analysis of Inorganic SEI Phases and a Methodology for Charge Correction. *ACS Appl. Energy Mater.* **2018**, *1*, 4493-4504.
(29) Wang, L.; Menakath, A.; Han, F.; Wang, Y.; Zavalij, P. Y.; Gaskell, K. J.; Borodin, O.; Iuga, D.; Brown, S. P.; Wang, C.; Xu, K.; Eichhorn, B. W. Identifying The Components of The Solid–electrolyte Interphase in Li-ion Batteries. *Nat. Chem.* **2019**, *11*, 789-796.
(30) Tasaki, K.; Goldberg, A.; Lian, J.-J.; Walker, M.; Timmons, A.; Harris, S. J. Solubility of Lithium Salts Formed on the Lithium-Ion Battery Negative Electrode Surface in Organic Solvents. *J. Electrochem. Soc.* **2009**, *156*, A1019 -A1027.
(31) Stetson, C.; Yin, Y.; Jiang, C.-S.; DeCaluwe, S. C.; Al-Jassim, M.; Neale, N. R.; Ban, C.; Burrell, A. Temperature-Dependent Solubility of Solid Electrolyte Interphase on Silicon Electrodes. *ACS Energy Lett.* **2019**, *4*, 2770-2775.

(32) Kern, W.; Puotinen, D. Cleaning Solutions Based on Hydrogen Peroxide for Use in Silicon Semiconductor Technology. *RCA Review* **1970**, *31*, 187-205.
(33) Zhuang, G. V.; Xu, K.; Yang, H.; Jow, T. R.; Ross, P. N. Lithium Ethylene Dicarbonate Identified as the Primary Product of Chemical and Electrochemical Reduction of EC in 1.2 M LiPF6/EC:EMC Electrolyte. *J. Phys. Chem. B* **2005**, *109*, 17567-17573.
(34) Schmid, M.; Steinrück, H.-P.; Gottfried, J. M., A New Asymmetric Pseudo-Voigt Function for More Efficient Fitting of XPS Lines. *Surf. Interface Anal.* **2014**, *46*, 505-511.

Table of Contents Graphic: